VSC Converter Feedback Control Data Optimization Based IGBT Collector Emitter Saturation Voltage Monitoring Through Nonlinear Least Squares Method

Yanjun Tian, *Member, IEEE*, Shaopeng Song, *Student Member, IEEE*, and Xiaoqi Xu, *Student Member, IEEE*

***Abstract*—Power switching device insulated gate bipolar transistor (IGBT) is a key component in the power conversion system (PCS). Fatigue-induced aging of its electrical characteristics can lead to serious degradation of PCS, such as increased losses and temperatures, fault shutdowns or equipment damage, even safety risks for the battery units. The collector-emitter saturation voltage V_{ce} is an essential indicator of IGBT health status, and the monitoring this ON-state saturation voltage can effectively assess its operational health. However, data-driven modeling-based monitoring algorithms are highly dependent on data quality and scale, and substandard data quality can cause significant deviations in the data model, besides extra sensors may not be feasible to be implemented on existing converters. To tackle these challenges, this article introduces a PCS feedback control data based nonlinear least squares curve fitting algorithm for the precise identification of the saturation voltage of IGBT. The PCS model has been established, which incorporate the IGBT dead-time switching character to enhance the accuracy. Additionally, for the collected feedback control data, a Kalman filter observer is constructed to reduce data deviations and noise interference, successfully mitigating the impact of sampling noise on identification accuracy. Finally, the correctness and effectiveness of the proposed IGBT ON-state saturations voltage monitoring method are verified through MATLAB/Simulink simulations and experimental setup.**

***Index Terms*—Condition monitoring, insulated gate bipolar transistor, Kalman filter, power conversion system.**

I. Introduction

TO ACHIEVE the goals of carbon peaking and carbon neutrality, it is essential to facilitate the multidirectional synergy among power generations, utility grids, loads, and energy storages to support renewable energy dominted electricity system [1]. Energy storage power stations can balance the power generations and demands, effectively improving the power system reliability. Power conversion system (PCS) is the key equipment in energy storage power sattions, serving as a critical bridge between the energy storage units and utility grid [2].

Insulated gate bipolar transistor (IGBT) is widely utilized as the crucial switching device in PCS, withstanding high voltage, and high switching frequencies. During switching process, the power losses cause junction temperature variations, and periodic fluctuations induce cyclic thermal stress changes. IGBT constructed materials have different thermal expansion coefficients, thus, the fluctuating thermal stress leads to certain mechanical separation of the bond wires and solder layers. Over time, this mechanical degradation gradually increases the contact resistance between different materials, resulting in elevated power losses, and temperature promotion, thus ultimately reduce the equipment reliability. This degradation seriously impacts the operating efficiency and safety of the PCS system. Therefore, monitoring the health status of IGBT operation is crucial for implementing timely and effective maintenance measures, enhancing the safe and stable operation of power electronic systems.

For the safe operation of energy storage power stations, the faults of PCS are typical high-risk factors. The fault of PCS can be classified as structural faults and parameter aging faults [3]. Structural faults are typically caused by electrical overstress, and this kind of fault impact can be mitigated through specific control strategies, such as fault diagnosis or fault tolerance control method. Parametric faults arise from wear and degradation in long-term operation and components deterioration, which can evolve into structural failures. Thus, PCS component condition monitoring is capable to evaluate the aging state and contribute predictive maintenance. Advancements in sensor accuracy and reliability, along with efficient modeling and data processing methods like digital twins, artificial intelligence (AI) and machine learning, now enable better monitoring of PCS physical models and internal parameters. These advancements strongly support the effective assessment of PCS equipment's lifespan, operational safety, and reliability [4].

According to industry survey data, approximately 20% of failures in power electronic systems are attributable to power semiconductor devices, making them one of the most failure-prone components [5]. The aging failure of IGBTs lead to changes in related electrical parameters. Currently, the ON-state voltage V_{ce} is recognized as a highly sensitive indicator for assessing IGBT aging [6].

Received 1 April 2025; revised 12 July 2025 and 28 August 2025; accepted 27 September 2025. Date of publication 9 October 2025; date of current version 13 November 2025. This work was supported in part by the National Key Research and Development Program of China under Grant 2023YFB2406800 and in part by the project and team of the Fundamental Research Funds for the Central Universities under Grant 2025MS113. Recommended for publication by Associate Editor G. De Carne. *(Corresponding author: Yanjun Tian.)*

The authors are with Yanzhao Electric Power Laboratory, North China Electric Power University, Baoding 071003, China (e-mail: yti@ncepu.edu.cn; songshaopeng@ncepu.edu.cn; xuxiaoqi@ncepu.edu.cn).

Color versions of one or more figures in this article are available at https://doi.org/10.1109/TPEL.2025.3616433.

Digital Object Identifier 10.1109/TPEL.2025.3616433

To achieve accurate monitoring of the ON-state voltage V_{ce}, a measurement circuit utilizing a metal-oxide-semiconductor field-effect transistor (MOSFET) as a switching element is proposed in [7]. However, this method requires additional hardware, significantly increasing cost. A monitoring circuit using a clamping setup with a reverse-series diode and Zener diode is proposed in [8]. Despite this, the circuit targets single-device measurements needing extra connection points, complicating its use in complex converter topologies. To solve this, a converter-level monitoring circuit is introduced, which connects directly to the midpoint of the converter bridge arm to measure the IGBT saturation voltage drop easily [9].

In large-scale energy storage power stations, the number of PCS units is numerous. Traditional monitoring methods require extra hardware, increasing costs, and complexity. Retrofitting existing systems with additional hardware is often impractical. Consequently, researchers globally have proposed methods that avoid the need for extra circuits. For example, the following conditions hold.

1) A fractional-order mathematical model of a Boost converter, combined with a particle swarm optimization (PSO) algorithm, has been used to enhance parameter identification accuracy [12].
2) Output voltage ripple data from converter trains a support vector machine to monitor and locate components faults [13].
3) Analysis of the dc-link capacitor discharge curve in traction converters leads to a proposed capacitor estimation method [14].

These approaches simplify condition monitoring without additional hardware, making them more practical for implementation.

In previous identification methods, IGBTs were considered ideal, ignoring their voltage drop and power loss during switching conduction. Previous identification methods treated IGBTs as ideal switches, ignoring their conduction characteristics. A Kalman filter–aided modular multilevel converters (MMC) monitoring scheme uses V_{ce} to formulate loop equations [15]. However, it is less effective in three-phase two-level PCS systems. This is due to voltage transients from inductive components.

With increased computing power, AI techniques are now more widely used in condition monitoring. For example, the following conditions hold.

1) A machine learning-based method monitors diodes forward voltage drop and MOSFET ON-state resistance of in dc–dc converters [16].
2) Backpropagation neural networks identify component parameters in dc–dc converters [17], though they require comprehensive offline training data.
3) A digital twin model with PSO algorithm for parameter identification has been developed for dc–dc converters [18], and extended to single-phase ac–dc converters [19].

These advancements aim to overcome limitations and improve the accuracy and applicability of condition monitoring techniques.

To effectively monitor the ON-state voltage of IGBTs in three-phase two-level converters, an accurate physical model is essential. Previous studies have modeled IGBTs in these converters as a voltage source in series with a resistor [20]. However, the ON-state voltage V_{ce} shows a linear relationship with the conduction current, according to IGBT output characteristic curves.

Despite progress, there is significant room for improving IGBT modeling accuracy, potentially through multiphysics simulation techniques. Additionally, many IGBT parameter identification studies use the PSO algorithm, which can be limited by tendencies to get stuck in local optima and sensitivity to parameter selection. The effectiveness of PSO, including convergence speed and search efficiency, heavily depends on the chosen parameters, often necessitating empirical tuning, and experimental validation for optimal results.

To address these limitations of PSO, alternative optimization algorithms have been explored. For instance, the whale optimization algorithm (WOA) demonstrates a stronger capability in avoiding local optima, offering advantages such as simpler implementation and faster convergence [29]. In contrast, AI-based algorithms typically require extensive training data and are often accompanied by higher computational complexity and greater resource demands [17]. The choice of optimization method significantly impacts the performance of parameter identification, which in turn plays a critical role in improving the accuracy of data-driven condition monitoring models. While methods in [18], [19], and [20] achieve IGBT condition monitoring, they do not consider measurement noise effects. Raw data quality is crucial, because sensor errors and noise can lead to inaccurate results [21].

The Kalman filter effectively reduces sampling noise and improves identification accuracy. In this study, multisensor data fusion combined with a Kalman filter is used during data acquisition. This method removes noise and increases monitoring precision for key parameters.

The rest of this article is organized as follows. Section II develops a mathematical model of the PCS, discusses the control and modulation methods, and explained the IGBT aging mechanisms and their impacts. Section III examines the effects of external factors on data and proposes a data preprocessing method. Section IV validates the proposed condition monitoring method through software simulations and experimental tests. Section V presents simulation and experiment verifications. Section VI presents discussions and potentials. Finally, Section VII concludes this article.

The main contributions of this article include the following.

1) *Effective Monitoring*: Utilizing PCS closed-loop control data and data-driven algorithms for effective IGBT saturation voltage monitoring.
2) *Nonintrusive Approach*: This method requires no additional sensors or hardware, reducing system complexity and cost.
3) *Accurate Aging Monitoring*: It precisely monitors key aging parameters of IGBTs, supporting robust predictive maintenance for the PCS.
4) *Improved Accuracy*: Theoretical analysis identifies inherent limitations in conventional monitoring approaches. By integrating multisensor data fusion with a Kalman filter to suppress measurement noise, the proposed method

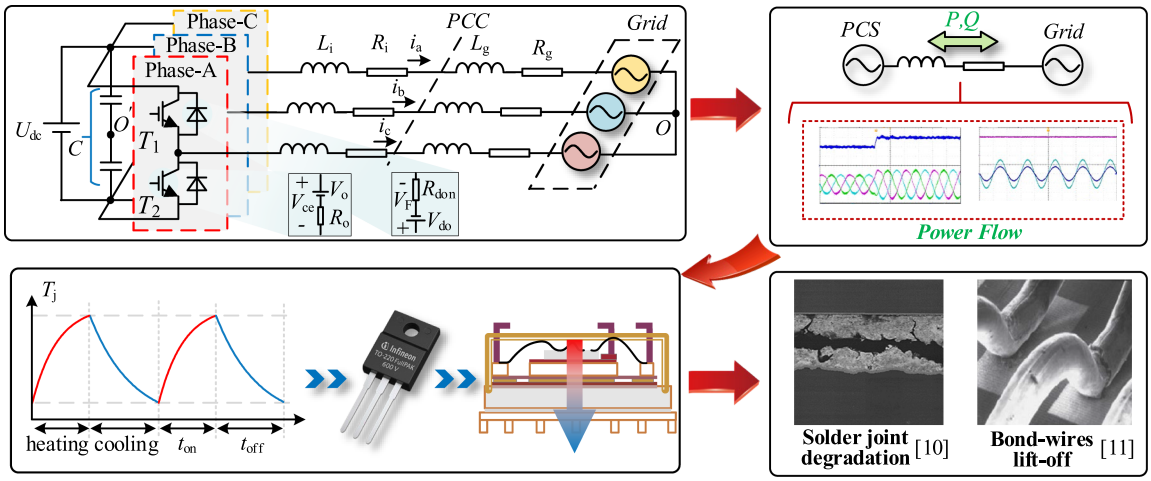

Fig. 1. Aging mechanism of IGBT.

achieves significantly improved condition monitoring accuracy.

II. IGBT On-State Voltage Fault Mapping and Monitoring Mechanism

A. Model of PCS

Fig. 1 shows the PCS topology, where U_{dc} represents the dc bus voltage, C denotes the dc filter capacitance, L_i is the filter inductance, R_i is the stray resistance of the filter inductance, and L_g and R_g are the inductance and resistance of the grid equivalent impedance, respectively. i_x (where x∈{a,b,c}) represent the three-phase grid-connected current, while e_x (where x∈{a,b,c}) denote three-phase grid voltage.

For easier analysis, the dc bus capacitor is represented as two series connected capacitors, with an imaginary midpoint O' marked. Using the circuit topology and Kirchhoff's voltage law, the mathematical equation of PCS three-phase voltage can be formulated as

$$\begin{cases} u_{ao'} = u_{ao} + u_{oo'} \\ u_{bo'} = u_{bo} + u_{oo'} \\ u_{co'} = u_{co} + u_{oo'}. \end{cases} \tag{1}$$

Based on the three-phase voltage balance of the grid-connected converter, it can be derived that

$$u_{ao} + u_{bo} + u_{co} = 0. \tag{2}$$

According to (1) and (2), $u_{o'o}$ can be expressed as

$$u_{o'o} = -\frac{1}{3} \cdot (u_{ao'} + u_{bo'} + u_{co'}). \tag{3}$$

Thus, the phase voltage can be reconstructed and expressed as

$$\begin{bmatrix} u_{ao} \\ u_{bo} \\ u_{co} \end{bmatrix} = \frac{1}{3} \begin{bmatrix} 2 & -1 & -1 \\ -1 & 2 & -1 \\ -1 & -1 & 2 \end{bmatrix} \cdot \begin{bmatrix} u_{ao'} \\ u_{bo'} \\ u_{co'} \end{bmatrix}. \tag{4}$$

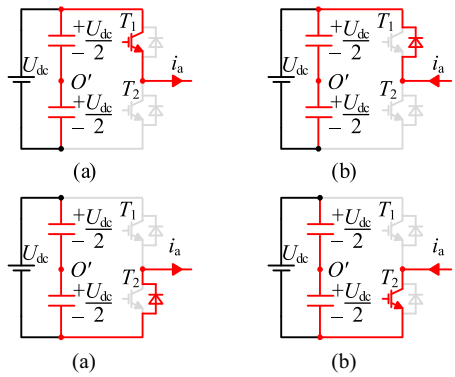

Fig. 2. Commutation circuit of PCS.

The three-phase output current of the PCS can be expressed as

$$\begin{bmatrix} \frac{di_a}{dt} \\ \frac{di_b}{dt} \\ \frac{di_c}{dt} \end{bmatrix} = \begin{bmatrix} \frac{1}{L_a} & 0 & 0 \\ 0 & \frac{1}{L_b} & 0 \\ 0 & 0 & \frac{1}{L_c} \end{bmatrix} \cdot \begin{bmatrix} u_{ao} - i_a \cdot R_a - e_a \\ u_{bo} - i_b \cdot R_b - e_b \\ u_{co} - i_c \cdot R_c - e_c \end{bmatrix} \tag{5}$$

where $L_x = L_i + L_g$ (where x ∈ {a,b,c}) represents the total inductance of the filter inductor and the grid-side inductor, and $R_x = R_i + R_g$ (where x ∈ {a,b,c}) represents the total resistance of the stray resistance of the filter inductor and the grid resistance.

As shown in Fig. 2, the conduction states of phase A in the PCS can be divided into four distinct modes, based on the IGBT conduction states and the direction of the grid-connected current. The switching function is defined as follows:

$$s = \begin{cases} 1 & \mathrm{T_1\ is\ on\ and\ T_2\ is\ off} \\ 0 & \mathrm{T_2\ is\ on\ and\ T_1\ is\ off} \end{cases}. \tag{6}$$

The PCS uses current closed-loop control in the d-q coordinate system, with a proportional integral (PI) controller to eliminate steady-state errors and adjust dynamic response speed, as shown in Fig. 3. i_{dref} and i_{qref} are dq-axis components of the reference grid-connected current, i_{gd} and i_{gq} are dq-axis components of feedback current. u_{tdref} and u_{tqref} are dq-axis

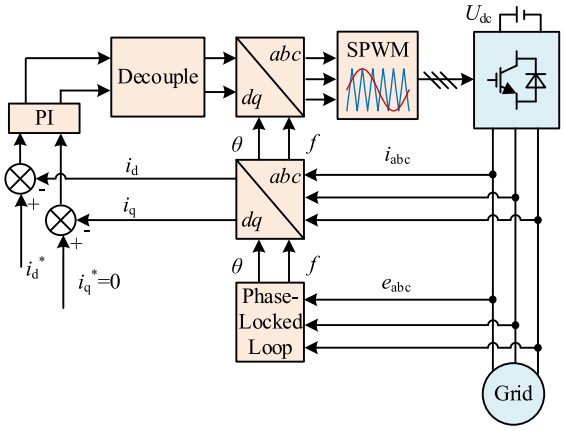

Fig. 3. Control strategy of PCS.

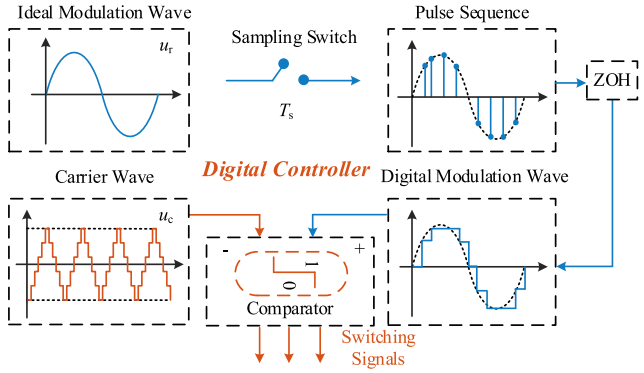

Fig. 4. Regular SPWM in digital control.

components of the output voltage on the PCS's ac side. The inner loop generates the sinusoidal fundamental voltage u_{dref} and u_{qref} on the PCS's ac side, and the modulated signal u_{abc} is produced via an inverse Park transform.

PCS modulation strategy employs bipolar sinusoidal pulsewidth modulation (SPWM), as shown in Fig. 4, which offers digital control with flexibility, adaptability, and robustness.

A digital signal processor (DSP) is normally applied for industrial PCS control, where a counter generates a stepped digital triangular carrier by cycling through addition and subtraction operations. This PWM wave controls the ON–OFF states of the IGBTs to produce the desired sinusoidal output.

Under normal conditions, the ON-state voltage V_{ce} of an IGBT can be expressed as

$$V_{\mathrm{ce}} = f(k_{\mathrm{a}}, T_{\mathrm{vj}}, V_{\mathrm{ge}}, I_{\mathrm{c}}) \tag{7}$$

where k_{a} denotes the aging factor, T_{vj} represents the junction temperature, and I_{c} is the ON-state collector current.

In practical applications, the influence of V_{ge} on V_{ce} can be neglected, as the parameters of the IGBT driver circuit and power supply are typically kept constant. Under fixed junction temperature conditions, the collector current I_{c} and the aging factor are the primary factors affecting V_{ce}. Therefore, IGBT ON-state saturation voltage V_{ce} and forward voltage V_{d} of antiparallel diode are positively correlated with the conducted current. These voltages need to be calculated based on identified values of V_{o}, V_{do}, R_{ON}, and R_{dON}. Fig. 1 shows the equivalent model of IGBT, where the ON-state voltage has a linear relationship with the current. The IGBT can be modeled as a resistor in series with a voltage source, and the ON-state voltage can be expressed as

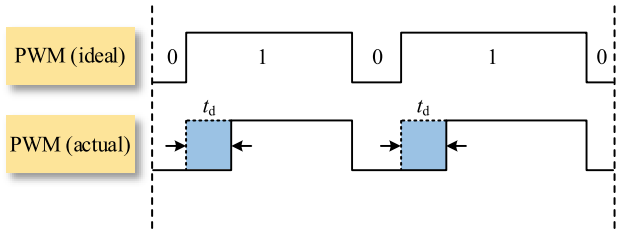

Fig. 5. Schematic diagram of trigger signal of the IGBT rising edge dead-time.

$$V_{\mathrm{ce}} = V_{\mathrm{o}} + I_{\mathrm{c}} R_{\mathrm{on}} \tag{8}$$

$$V_{\mathrm{F}} = V_{\mathrm{do}} + I_{\mathrm{d}} R_{\mathrm{don}} \tag{9}$$

where V_{o} and R_{ON} are IGBT threshold voltage and equivalent resistance, respectively, V_{do} and R_{dON} are, respectively, antiparallel diode threshold voltage and equivalent resistance, I_{c} is IGBT collector current, and I_{d} is the antiparallel diode current. Thus, the accurate phase voltage can be expressed as

$$\begin{aligned} u_{\mathrm{ao}} &= u_{\mathrm{ao'}} + u_{\mathrm{o'o}} \\ &= (2s-1)\frac{U_{\mathrm{dc}}}{2} + s \cdot (\mathrm{sign}(i_{\mathrm{a}}) \cdot (-V_{\mathrm{ce1}}) + \overline{\mathrm{sign}(i_{\mathrm{a}})} \cdot V_{\mathrm{F1}}) \\ &\quad + \overline{s} \cdot (\overline{\mathrm{sign}(i_{\mathrm{a}})} \cdot (V_{\mathrm{ce2}}) + \mathrm{sign}(i_{\mathrm{a}}) \cdot (-V_{\mathrm{F2}})) + u_{\mathrm{o'o}} \end{aligned} \tag{10}$$

where sign (i_{a}) represents the direction of the current. When the current flows from PCS to the power grid, sign (i_{a}) is 1, otherwise it is 0. The variable s denotes the ON and OFF states of the IGBT.

To enhance the model's accuracy, consider the delay in the digital control system. This article accounts for the IGBT ON–OFF dead zone time, t_{d}. As Fig. 5 shows, the rising edge of the IGBT gate drive signal is delayed by t_{d}. The falling edge signal stays unchanged.

B. Aging Mechanisms and Characterization Analysis of IGBT

The monitoring of IGBTs utilizes both thermal and electrical signals. Thermal signal monitoring is less invasive and easier to implement. However, housing temperature can be easily interfered with by other heat sources, such as adjacent power modules and components, and ambient temperature, showing low degradation sensitivity.

In contrast, the electric parameter method features rapid response and strong online application capability. The ON-state resistance R_{ON} includes the resistance of the semiconductor chip, bond-wire, copper trace wire, and connection terminal. It is expressed as

$$R_{\mathrm{on}} = R_{\mathrm{chip}} + R_{\mathrm{bond}} + R_{\mathrm{copper}} + R_{\mathrm{term}} \tag{11}$$

where R_{chip}, R_{bond}, R_{copper}, and R_{term} represent the resistances of the semiconductor chip, bond wires, copper trace wires, and connecting terminals, respectively.

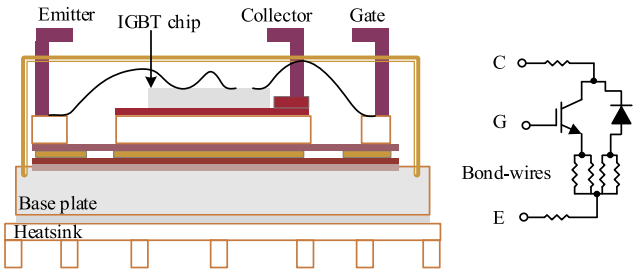

Fig. 6. Electrical characteristics change with IGBT aging.

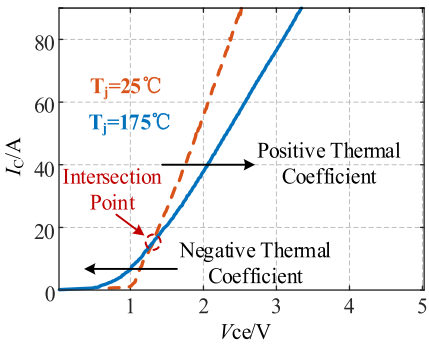

Fig. 7. Output characteristic of IGBT.

The IGBT module's structure is illustrated in Fig. 6. Mismatch in thermal expansion coefficients generates thermal stress, impacting the device's reliability during long-term thermal cycling or power cycling. As shown in the figure, the bond wires are connected in parallel. When a bond wire breaks, the total equivalent resistance increases, as indicated by (8) and (11). This increase leads to a rise in the ON-state voltage.

Aging of the solder layer reduces the IGBT's heat dissipation performance and increases thermal resistance. This leads to a higher junction temperature, resulting in a reduction in saturation voltage [22]. Consequently, the ON-state voltage is highly sensitivity to the degradation of power semiconductors and is commonly used to characterize the degree of aging of IGBTs. During the power cycling, the ON-state voltage V_{ce} of IGBT increases with aging.

Fig. 7 shows the output characteristic curve of an IGBT in a healthy state. It can be observed that the output characteristic curves at different temperatures intersect at a knee point. When the conduction current is fixed, the portion of the curve above the knee point shows a positive correlation between ON-state voltage and junction temperature, while the portion below the knee point exhibits a negative correlation. At the knee point itself, the ON-state voltage is independent of the junction temperature. After identifying the ON-state voltage V_{ce}, use the manufacturer's datasheet to find the saturation voltage drop in a healthy state. Compare the identified ON-state voltage with the healthy state to evaluate IGBT aging. This article focuses on methods for identifying the ON-state voltage of IGBTs.

C. Existing Condition Monitoring Techniques for IGBTs

Table I summarizes typical condition monitoring methods for IGBTs. Hardware measurement methods require additional hardware and are somewhat invasive. Data processing methods are noise-sensitive and computationally intensive.

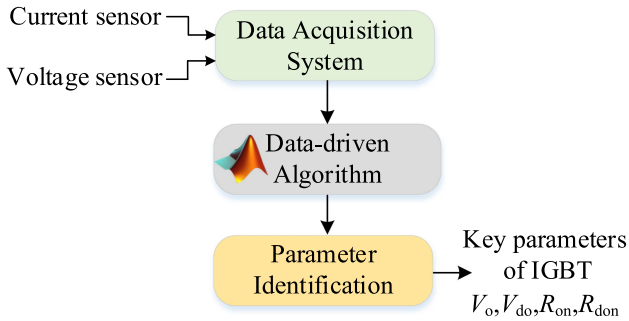

Fig. 8. Flowchart of parameter identification.

In previous studies on modeling three-phase two-level converters, parasitic parameters of power devices were often overlooked or not accurately modeled. Devices were typically treated as ideal switches.

The PSO algorithm is commonly used for identifying parasitic parameters but can get stuck in local optima. It is sensitive to parameter settings such as velocity inertia weight (ω) and learning factors (c_1 and c_2), which affect convergence speed and search effectiveness. These parameters need careful adjustment based on experience and experimentation for optimal results. Moreover, prior research has not adequately accounted for the impact of data quality on parameter identification.

Fig. 8 presents a flow chart of the parameter identification process. Key challenges include data accuracy, external noise, data drift, bad data, and dynamic insufficiency.

The accuracy of data directly affects the credibility of research results. Previous studies often lack data optimization processing. They also have high demands regarding data scale and working conditions. Therefore, during the data handling process, data accuracy is crucial for credible results. Many studies do not adequately optimize their data, and there are significant requirements for the scale and conditions of the data. To ensure data reliability and validity during the identification process, it is essential to implement strict preprocessing, filtering, and model optimization. Addressing the mentioned issues, this article introduces an identification method that integrates data optimization with the least squares approach. This method offers several advantages, such as enhanced identification accuracy, reduced computational complexity, and decreased reliance on large datasets.

D. Mechanism of Faulty Data Generation and Impact Analysis

Data quality is vital for the accuracy of parameter identification. If the original data is not ideal, significant errors can occur. Fig. 9 analyzes the factors affecting data accuracy. Hall sensors are commonly used for data sampling in converters. Their measurement accuracy can be impacted by: electromagnetic interference, switching frequency ripple, and sampling frequency. These factors may cause the identification results to deviate from the true values.

TABLE I
COMPARISON OF DIFFERENT POWER DEVICE CONDITION MONITORING METHODS

Ref.	Classification	Applications	Health indicators	Noise immunity	Additional sensors	Algorithm complexity	Accuracy	Special operation	Experimental Validation
[7]	V_{ce} Measurement	DC-DC Converters	ON-state voltage	High	Yes	Low	High	Yes	Physical Experiment
[15]	KVL modeling with linear solving	MMC	ON-state voltage	High	No	Low	High	No	Simulation Only
[16]	Physics-informed machine learning	DC-DC Converters	ON-state Resistance	High	No	High	High	No	Physical Experiment
[17]	Backpropagation neural network	DC-DC Converters	ON-state Resistance	High	No	High	High	No	Physical Experiment
[19]	PSO	PWM Rectifiers	ON-state voltage	Low	No	Medium	High	No	Physical Experiment
[25]	Junction temperature measurement	Any IGBTs applications	Thermal	High	Yes	Low	Medium	No	Physical Experiment
[26]	Transient characteristic measurement	Any IGBTs applications	Miller plateau, Switching delay, Gate current···	Low	Yes	Low	High	Yes	Physical Experiment
[27]	PSO	ANPC Inverters	ON-state voltage	Low	No	Medium	High	No	Physical Experiment
[28]	Model-based	DC-AC Converters	ON-state voltage	Medium	No	Low	High	No	Hardware-in-the-loop
Proposed	TRRLS+Kalman	DC-AC Converters	ON-state voltage	High	No	Low	High	No	Physical Experiment

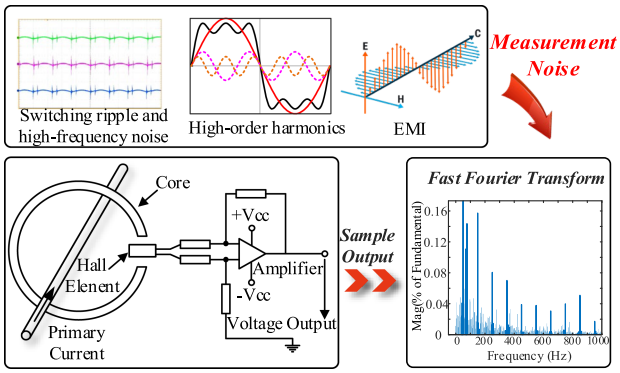

Fig. 9. Data accuracy impact analysis.

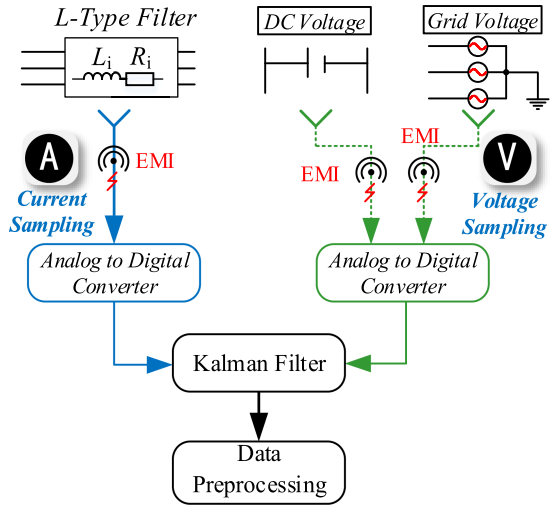

Fig. 10. Flowchart of data sampling.

Sensor errors and noise interference can cause identification results to deviate from true values, leading to model mismatch. Bad data and outliers may prevent the algorithm from converging, or cause it to converge to local optima. This reduces identification efficiency. Moreover, such poor-quality data increase the computational burden and waste computing resources.

III. DATA ACQUISITION AND PREPROCESSING

A. Data Acquisition

In the PCS control system, the electrical signal measurement process is shown in Fig. 10. After the current and voltage signals are captured by respective sensors, they are transmitted into the controller as voltage signals. Within the dSPACE system, these signals undergo analog-to-digital (A/D) conversion. After conversion, the signals are amplified and restored to their true values. The processed signals are then utilized for closed-loop control and parameter identification, ensuring precise control and efficient operation of the system.

B. Data Preprocessing

Considering the impact of bad data on identification accuracy, this article adopts multisensor data fusion to enhance information exchange between sensors. It leverages the Kalman optimization algorithm for real-time recursive filtering in data preprocessing. Using system operation data collected by the sensor, such as dc side voltage, junction voltage, and current, the Kalman filter algorithm can accurately estimate the electrical signal from the noisy measurement data. It effectively eliminates sensor-induced measurement noise. The algorithm reduces

uncertainty disturbances and improves current measurement accuracy.

The Kalman filter algorithm operates in two phases: 1) prediction and 2) correction. The steps to establish a Kalman filter are as follows:

$$L_{\mathrm{x}}\frac{i_{\mathrm{x}}(t_{\mathrm{k}})-i_{\mathrm{x}}(t_{\mathrm{k-1}})}{T_{\mathrm{sa}}}=u_{\mathrm{xo}}-R_{\mathrm{x}}\cdot i_{\mathrm{x}}(t_{\mathrm{k-1}})-e_{\mathrm{x}} \tag{12}$$

where $i(t_{\mathrm{k}})$ and $i(t_{\mathrm{k\text{-}1}})$ represent the current value at time instants t_{k} and $t_{\mathrm{k\text{-}1}}$, respectively, T_{sa} is the sampling period, i.e., $T_{\mathrm{sa}}=t_{\mathrm{k}}\text{-}t_{\mathrm{k\text{-}1}}$, and x∈{a,b,c}

$$\begin{cases}\boldsymbol{x}_k=\boldsymbol{A}\boldsymbol{x}_{k-1}+\boldsymbol{B}\boldsymbol{u}_{k-1}+\boldsymbol{w}_k\\ \boldsymbol{y}_k=\boldsymbol{C}\boldsymbol{x}_k+\boldsymbol{v}_k.\end{cases} \tag{13}$$

Associate with (12), the state equation of the system can be defined as

$$\boldsymbol{A}=\boldsymbol{I}-T_{\mathrm{sa}}\cdot\begin{bmatrix}\frac{R_{\mathrm{a}}}{L_{\mathrm{a}}}&0&0\\0&\frac{R_{\mathrm{b}}}{L_{\mathrm{b}}}&0\\0&0&\frac{R_{\mathrm{c}}}{L_{\mathrm{c}}}\end{bmatrix}$$

$$\boldsymbol{B}=T_{\mathrm{sa}}\cdot\begin{bmatrix}\frac{1}{L_{\mathrm{a}}}&0&0\\0&\frac{1}{L_{\mathrm{b}}}&0\\0&0&\frac{1}{L_{\mathrm{c}}}\end{bmatrix}$$

$$\boldsymbol{C}=\boldsymbol{I},\boldsymbol{v}=10^{-6}\cdot\boldsymbol{I},\omega=\boldsymbol{0}$$

where $\boldsymbol{I}$ represents the identity diagonal matrix.

Then, based on (13), state variable predicted value can be calculated as

$$\hat{\boldsymbol{x}}_{\mathrm{n}}^{-}=\boldsymbol{A}\hat{\boldsymbol{x}}_{\mathrm{n-1}}+\boldsymbol{B}\boldsymbol{u}_{\mathrm{n}}. \tag{14}$$

Based on the *a posteriori* error matrix $\boldsymbol{P}_{\mathrm{n\text{-}1}}$, the *a priori* error covariance matrix equation can be derived as

$$\boldsymbol{P}_{\mathrm{n}}^{-}=\boldsymbol{A}\boldsymbol{P}_{\mathrm{n-1}}\boldsymbol{A}^{T}+\boldsymbol{Q} \tag{15}$$

where $\boldsymbol{Q}$ represents the process noise covariance matrix

$$\boldsymbol{K}_{\mathrm{n}}=\boldsymbol{P}_{\mathrm{n}}^{-}\boldsymbol{C}^{T}\left(\boldsymbol{C}\boldsymbol{P}_{\mathrm{n}}^{-}\boldsymbol{C}^{T}+\boldsymbol{R}\right)^{-1} \tag{16}$$

where $\boldsymbol{R}$ is the measurement noise covariance matrix.

Subsequently, the optimal estimate can be calculated as

$$\hat{\boldsymbol{x}}_{\mathrm{n}}=\hat{\boldsymbol{x}}_{\mathrm{n}}^{-}+\boldsymbol{K}_{\mathrm{n}}\left(\boldsymbol{y}_{\mathrm{n}}-\boldsymbol{C}\hat{\boldsymbol{x}}_{\mathrm{n}}^{-}\right) \tag{17}$$

where y_{n} is the measured variable value.

Finally, the error covariance matrix $\boldsymbol{P}_{\mathrm{n}}$ is updated to compute the priori error covariance estimate for the next time step. This update, can be expressed as

$$\boldsymbol{P}_{\mathrm{n}}=\left(\boldsymbol{I}-\boldsymbol{K}_{\mathrm{n}}\boldsymbol{C}\right)\boldsymbol{P}_{\mathrm{n}}^{-} \tag{18}$$

where $\boldsymbol{I}$ is the identity diagonal matrix.

Once the PCS stable operation data is obtained, the measurement data from the sensors are fused. The actual values for the closed-loop control data are then estimated using the Kalman filter algorithm.

IV. IGBT Saturation Voltage Identification Through Nonlinear Least Squares

In practical applications, dead time is included in the modulation process to prevent simultaneous conduction of the upper and lower power IGBTs. Nonideal characteristics like the ON-state voltage of IGBT and switching delay introduce nonlinearity into the converter's operation. Traditional linear identification methods are inadequate for fully capturing the system's dynamic behavior. To address these issues, nonlinear algorithms are necessary for accurately identifying the inverter's complex nonlinear behaviors. This article proposes a nonlinear least squares curve fitting approach for IGBT parameter identification. It integrates Kalman filtering to reduce noise impact during condition monitoring. These enhancements aim to simplify debugging complexity and improve the algorithm's robustness and applicability.

A. PCS Mathematical Analytical Model

To establish a mathematical analytical model for curve fitting using the state equation, it is necessary to discretize the differential equation. The Runge–Kutta method is widely used for solving differential equations and offers several advantages [23]: It uses a recursive approach to find numerical solutions. It provides high accuracy and is straightforward to implement. The inductive current at the next sampling interval can be expressed as

$$\begin{cases}i_{\mathrm{a,n+1}}=i_{\mathrm{a,n}}+\frac{h}{6}\cdot\left(k_{\mathrm{a1}}+2k_{\mathrm{a2}}+2k_{\mathrm{a3}}+k_{\mathrm{a4}}\right)\\ i_{\mathrm{b,n+1}}=i_{\mathrm{b,n}}+\frac{h}{6}\cdot\left(k_{\mathrm{b1}}+2k_{\mathrm{b2}}+2k_{\mathrm{b3}}+k_{\mathrm{b4}}\right)\\ i_{\mathrm{c,n+1}}=i_{\mathrm{c,n}}+\frac{h}{6}\cdot\left(k_{\mathrm{c1}}+2k_{\mathrm{c2}}+2k_{\mathrm{c3}}+k_{\mathrm{c4}}\right)\end{cases} \tag{19}$$

where i_{a}, i_{b}, and i_{c} are phase currents

$$\begin{cases}\left[k_{\mathrm{a1}},k_{\mathrm{b1}},k_{\mathrm{c1}}\right]=f\left(a_{\mathrm{n}},b_{\mathrm{n}},c_{\mathrm{n}}\right)\\ \left[k_{\mathrm{a2}},k_{\mathrm{b2}},k_{\mathrm{c2}}\right]=f\left(a_{\mathrm{n}}+\frac{h}{2}k_{\mathrm{a1}},b_{\mathrm{n}}+\frac{h}{2}k_{\mathrm{b1}},c_{\mathrm{n}}+\frac{h}{2}k_{\mathrm{c1}}\right)\\ \left[k_{\mathrm{a1}},k_{\mathrm{b3}},k_{\mathrm{c3}}\right]=f\left(a_{\mathrm{n}}+\frac{h}{2}k_{\mathrm{a2}},b_{\mathrm{n}}+\frac{h}{2}k_{\mathrm{b2}},c_{\mathrm{n}}+\frac{h}{2}k_{\mathrm{c2}}\right)\\ \left[k_{\mathrm{a4}},k_{\mathrm{b4}},k_{\mathrm{c4}}\right]=f\left(a_{\mathrm{n}}+\frac{h}{2}k_{\mathrm{a3}},b_{\mathrm{n}}+\frac{h}{2}k_{\mathrm{b3}},c_{\mathrm{n}}+\frac{h}{2}k_{\mathrm{c3}}\right)\end{cases} \tag{20}$$

where $f=[di_{\mathrm{a}}/dt,\ di_{\mathrm{b}}/dt,\ di_{\mathrm{c}}/dt]$, h is the time step between the nth and $(n+1)$th sampling points, and k is the average slope rate between the nth and $(n+1)$th sampling points

$$\begin{bmatrix}i_{\mathrm{a,n+1}}\\i_{\mathrm{b,n+1}}\\i_{\mathrm{c,n+1}}\end{bmatrix}=f(V_{oi},R_{\mathrm{on}i},V_{\mathrm{d}i},R_{\mathrm{don}i})\cdot\begin{bmatrix}i_{\mathrm{a,n}}\\i_{\mathrm{b,n}}\\i_{\mathrm{c,n}}\end{bmatrix}. \tag{21}$$

In this article, the IGBT parasitic parameters are identified using the least squares method based on trust region reflection, in conjunction with the previously described converter mathematical analysis model.

B. Trust-Region Reflective Nonlinear Least Squares

Trust-region reflective nonlinear least squares (TRRLS) is an effective method for solving nonlinear minimization problems with constrained bounds [24]. Specifically, TRRLS is used to

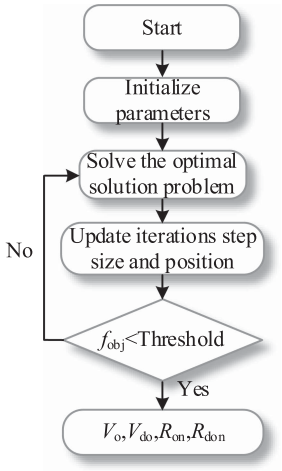

Fig. 11. Flowchart of parameter identification.

determine the coefficient x that solve the following problem:

$$\min_x \|F(x, x\text{data}) - y\text{data}\|_2^2 = \min_x \sum_i (F(x, x\text{data}_i) - y\text{data}_i)^2. \tag{22}$$

In the equation, $x$data denotes the given input data, $y$data represents the observed output, and $F(x, x\text{data})$ is a matrix-valued or vector-valued function of the same size as $y$data.

$$f_{\text{obj}} = \sum_i (F(x, x\text{data}_i) - y\text{data}_i)^2. \tag{23}$$

TRRLS uses a quadratic function $q(s)$ to approximate the objective function $f_{\text{obj}}(x)$. By minimizing $q(s)$ within a neighborhood N, the search step s is computed such that the next iteration point $x+s$ corresponds to a local minimum. This ensures global convergence. The basic form of the method is as follows:

$$\left.\begin{aligned} \min_s\{q_{\text{k}}(s) : \|\boldsymbol{D}_{\text{k}} s\|_2 \le \Delta_{\text{k}}\} \\ q_{\text{k}}(s) = \tfrac{1}{2} s \boldsymbol{H}_{\text{k}} s + s^{\text{T}} g_{\text{k}} \end{aligned}\right\} \tag{24}$$

where s is the search step, $\boldsymbol{H}_{\text{k}}$ is the Hessian matrix, $\boldsymbol{D}_{\text{k}}$ is the diagonal scale matrix, Δk is the trust region scale, and g_{k} is the gradient of $f_{\text{obj}}(x)$.

If $f_{\text{obj}}(x_{k+1}) < f_{\text{obj}}(x_k)$, then $x_{\text{k}+1} = x_{\text{k}} + \alpha_{\text{k}} s_{\text{k}}$, α_{k} is limited by the boundary. The reflection trust region method will "reflect" the solution back to the trust region, thereby avoiding invalid solutions and continuing the optimization process; Otherwise, the iteration point remains unchanged and the trust region is further reduced. The flow chart of nonlinear least square method is shown in Fig. 11.

By substituting experimental measurement data (t_1, i_1), $(t_2, i_2), \ldots, (t_{\text{j}}, i_{\text{j}})$ and mathematical model calculation data into (25), the unknown parameter variables in the function can be determined using the criterion of minimizing the loss function.

TABLE II
SIMULATION PARAMETERS

Parameters	Value	Parameters	Value
DC Voltage U_{dc}	400 V	DC-Link Capacitor C	800 μF
Grid voltage V_{g}	110 V	Line resistance R_{g}	0.1 Ω
Filter inductance L_{i}	4 mH	Sampling frequency f_{sa}	1×10^6Hz
Spurious resistance R_{i}	0.5 Ω	Calculation step size h	1×10^{-6} s
Line inductance L_{g}	1 mH	ON-state resistance R_{on}	0.15 Ω
Threshold voltage V_{o}	1.5 V	ON-state resistance R_{don}	0.02 Ω
Threshold voltage V_{do}	1 V	Switching frequency f_{sw}	10 kHz

In this article, the objective function of the algorithm is defined as

$$f_{obj} = \frac{\sum_{j=1}^{N} \left[(i_{\text{a},j} - i_{\text{am},j})^2 + (i_{\text{b},j} - i_{\text{bm},j})^2 + (i_{\text{c},j} - i_{\text{cm},j})^2\right]}{N}. \tag{25}$$

By fitting the experimental three-phase grid-connected current waveform data using (25), the ON-state resistance and threshold voltage of IGBT can be determined.

V. SIMULATION AND EXPERIMENT VERIFICATIONS

A. Simulation

Fig. 12 illustrates the TRRLS algorithm-based IGBT parameter monitoring block diagram. To ensure the accuracy of parameter identification, the input data is selected from the steady-state operation phase of the energy storage converter. A typical sampling time window ranges from 50 ms to 80 ms, covering multiple fundamental periods and including several IGBT conduction intervals. This ensures both the stability and representativeness of the data used in the identification process. First, the collected data is converted from analog to digital using dSPACE. To improve the accuracy of parameter identification, the sampling noise needs to be filtered, the actual data collected by the sensor is processed using the Kalman filter algorithm, and then the preprocessed data of sensor acquisition and closed-loop control are substituted into the mathematical analytical model. Finally, the TRRLS algorithm is applied for curve fitting to obtain the IGBT aging characteristic parameters.

The PCS grid-connected system simulation model, illustrated in Fig. 1, was developed using MATLAB/Simulink software, with the simulation parameters detailed in Table II. In the simulation, the inductors and resistors are modeled using the Three-Phase Series *RLC* Branch block in Simulink. The IGBT is implemented by connecting an IGBT block in parallel with a Diode block, allowing for accurate representation of the device's switching behavior. Key parameters such as threshold voltage and on-state resistance can be configured to reflect the conduction characteristics of the actual device.

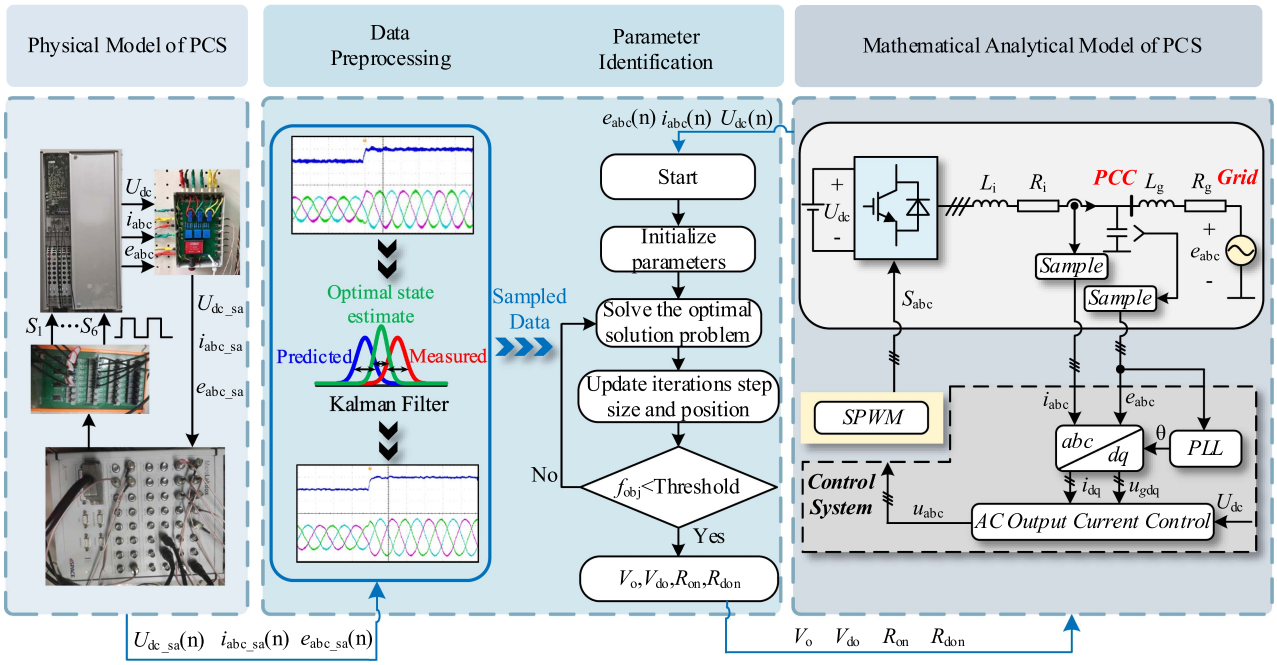

Fig. 12. Diagram of TRRLS-based IGBT parameter monitoring.

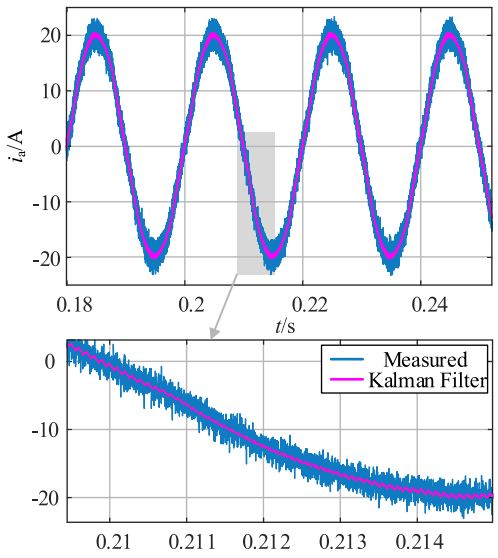

Fig. 13. Comparison of measured values and Kalman filter estimates.

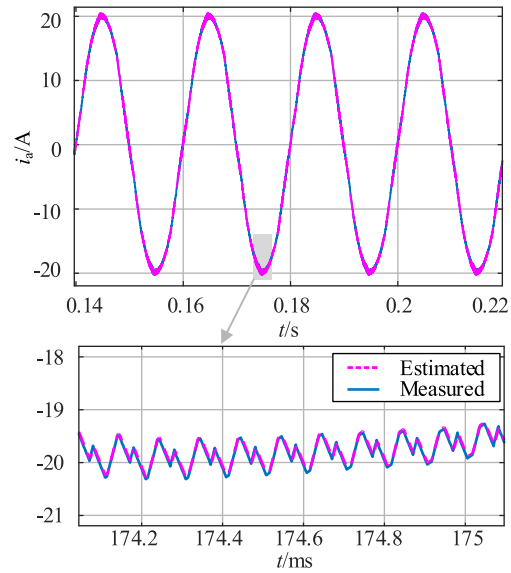

Fig. 14. Comparison of current waveforms between simulation and mathematical model.

To simulate practical noise impact, broadband white noise was injected into sensor signals. As shown in Fig. 13, the Kalman filter effectively reduces measurement noise and maintains high accuracy.

Fig. 14 compares the phase-A grid-connected current in the PCS between the simulation model under steady-state operation and the mathematical analytical model using the NLS-TRRLS method. As shown, the output characteristics of the two models are nearly identical, indicating high modeling accuracy and validating the effectiveness of the condition monitoring method in achieving precise identification.

Table III presents the 10 identification results of the IGBT in the PCS. The monitoring results show that the estimated parameters are very close to the simulation setpoints, demonstrating that the proposed condition monitoring algorithm can effectively track the aging parameters of the IGBT. Although R_{ON} and R_{dON} have relatively large identification errors, their impact on the overall ON-state voltage is small. Therefore, this larger error is acceptable.

To clearly illustrate the distribution characteristics of the monitored parameters, Fig. 15 utilizes a boxplot to compare the identification results of IGBT characteristic parameters before

TABLE III
MONITORING RESULTS OF IGBT KEY PARAMETERS

Number	V_{o1}(V)	V_{do1}(V)	R_{on1}(Ω)	R_{don1}(V)	V_{o2}(V)	V_{do2}(V)	R_{on2}(Ω)	R_{don2}(Ω)
1	1.5644	0.9773	0.1587	0.0181	1.5189	0.9750	0.1416	0.0196
2	1.5048	0.9593	0.1539	0.0208	1.5048	0.9573	0.1555	0.0211
3	1.4862	0.9713	0.1376	0.0184	1.4862	1.0457	0.1417	0.0216
4	1.5289	1.0005	0.1513	0.0212	1.5289	1.0005	0.1624	0.0190
5	1.4332	0.9864	0.1485	0.0198	1.4898	1.0457	0.1545	0.0207
6	1.5309	1.0436	0.1507	0.0189	1.5309	1.0486	0.1444	0.0186
7	1.4960	0.9682	0.1598	0.0219	1.4960	0.9715	0.1596	0.0204
8	1.5181	0.9562	0.1624	0.0203	1.5048	0.9924	0.1442	0.0212
9	1.5253	1.0397	0.1564	0.0207	1.5253	1.0345	0.1496	0.0207
10	1.4857	1.0394	0.1503	0.0193	1.4898	1.0394	0.1455	0.0183
Average	1.5074	0.9942	0.1530	0.0199	1.5075	1.0111	0.1499	0.0201
Setpoint	1.5	1	0.15	0.02	1.5	1	0.15	0.02
Max Err	4.45%	4.38%	8.27%	9.50%	2.06%	4.86%	8.26%	8.50%

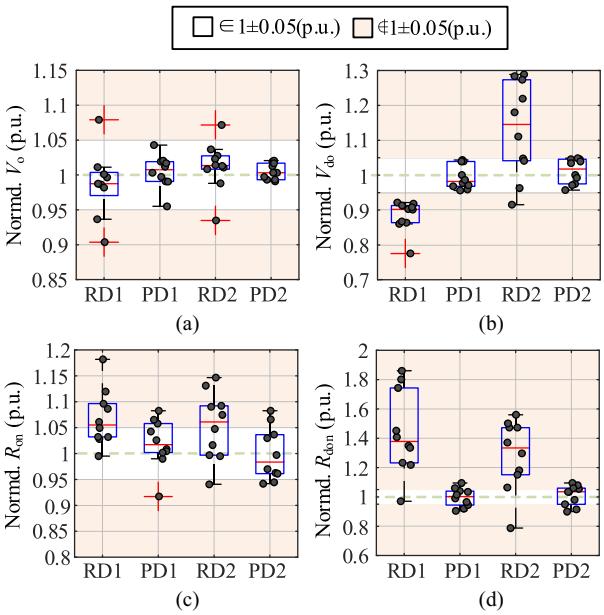

Fig. 15. Identifying data distribution characteristics.

and after data processing. In the boxplot, the width of the box reflects the degree of data dispersion. The results indicate that the identification raw data (RD) contains outliers and exhibits significant deviations from the set values, whereas the identification with processed data (PD) is more tightly clustered and closely aligns with the set values. This confirms that the proposed identification algorithm demonstrates high precision and stability.

Considering the influence of various factors in the actual sampling process, the simulated data features verify three aspects of interference besides adding white noise to the data: analog-to-digital converter quantization error, noise susceptibility, and synchronization error. The algorithm's performance was evaluated under different test conditions. Results show that the method achieves high parameter identification accuracy in interference-free cases. Even with added disturbances, the estimation errors remain low, indicating good accuracy and robustness. This analysis confirms that the proposed condition monitoring algorithm has strong anti-interference capability. It also reduces the need for large-scale, high-quality data, showing good potential for engineering applications.

TABLE IV
SYSTEM PARAMETERS

Parameters	Value	Parameters	Value
DC Voltage U_{dc}	400 V	Switching frequency f_{sw}	10 kHz
Grid voltage V_g	110 V	Line resistance R_g	0.1 Ω
Filter inductance L_i	4 mH	Sampling frequency f_{sa}	20 kHz
Spurious resistance R_i	0.1 Ω	Calculation step size h	1×10^{-6} s
Line inductance L_g	1 mH	Fundamental frequency f_c	50 Hz
Dead time t_d	2 μs	IGBT module	IHW30N120R5

B. Experiment

To further validate the accuracy and effectiveness of the monitoring method, a PCS experimental platform was built. The experimental parameters were provided in Table IV, and the experimental platform was depicted in Fig. 16. In the experiment, the parasitic resistance R_i of the filter inductor can be obtained either through the identification algorithm proposed in this article or by using a precision LCR meter available in the laboratory. Due to the presence of grid impedance, the measurable voltage on the inverter side is the point of common coupling voltage, while the grid voltage cannot be directly measured. To address this issue, the grid voltage information is indirectly derived using a parallel capacitor, as illustrated in Fig. 12. By combining the capacitor voltage with the loop voltage equation, the inductor voltage drop is calculated. This enables the estimation of the inductor current, which is further used to identify the IGBT saturation voltage drop. The accuracy of the identified model is verified by comparing the output current from the model with

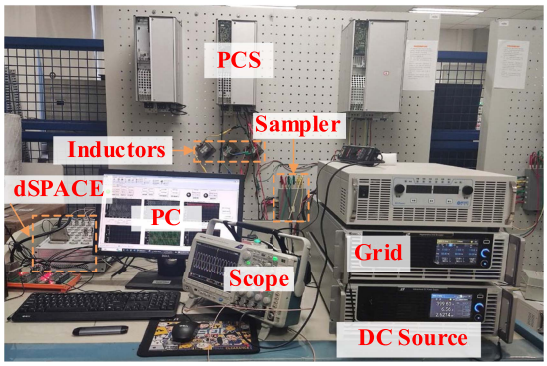

Fig. 16. Experimental platform.

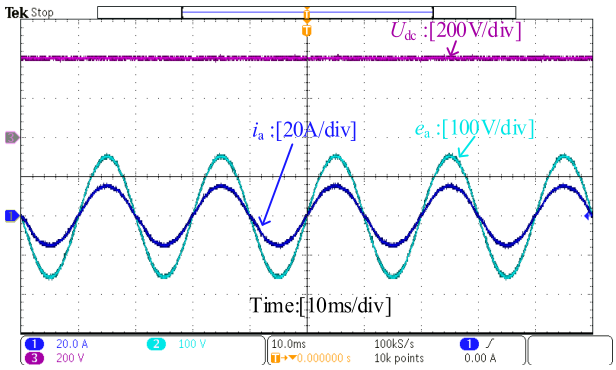

Fig. 17. Waveforms of the PCS in steady state.

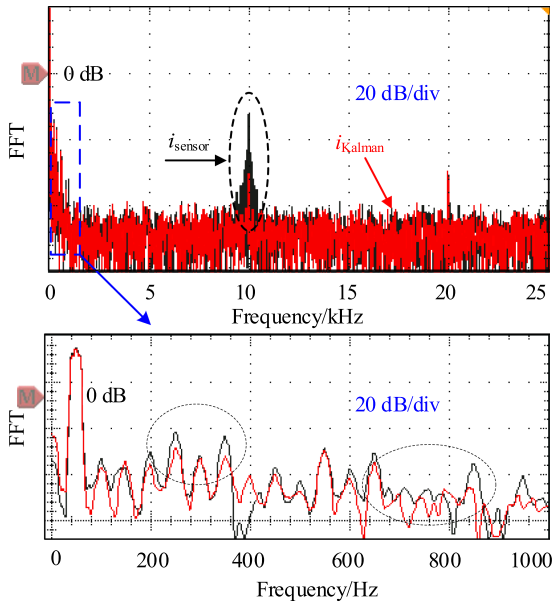

Fig. 18. Comparison and harmonic analysis of Kalman-filtered current and measured current.

that of the actual system. The proposed method does not require prior knowledge of the grid impedance and is insensitive to its influence.

The PCS was implemented using a Danfoss converter, while the control unit utilized a dSPACE Micro-LabBox 1202 real-time controller. During operation, the sampling circuit captures electrical signals and transmits them to the controller. The dSPACE platform then converts these analog signals into digital format and generates PWM signals in the form of optical signals to control the switching of IGBTs, enabling closed-loop control.

The ON-state voltage of both IGBTs and antiparallel diodes is influenced by temperature. Therefore, data must be collected immediately after each startup of the PCS to ensure a constant temperature is maintained. To minimize the impact of junction temperature variation on measurement accuracy, this study uses the SMART SENSOR ST9550—a high-precision junction temperature measurement device. The IGBT module is measured directly with the housing panel of the PCS opened. This approach effectively improves measurement accuracy, reduces temperature deviations during repeated tests, and enhances the stability and repeatability of the parameter extraction results.

Fig. 17 shows the steady-state operation waveform of PCS when they are connected to the grid. As shown, the current and voltage are in phase, and the PCS operates at a unit power factor.

The comparison of the Kalman filter output with the sensor-measured current and the harmonic analysis results are presented in Fig. 18. As shown, the Kalman filter demonstrates remarkable effectiveness in eliminating higher order harmonics, while simultaneously suppressing low-order harmonics in the current signal, thereby significantly enhancing identification accuracy. It should be noted that the noise reduction effect of the Kalman filter in this experiment is limited, and only minor differences are observed between the signals before and after filtering. The fast Fourier transform results presented in the article are mainly used to visualize the time-domain waveforms before and after filtering. The small discrepancies may be attributed to noise introduced during the digital-to-analog converter playback and oscilloscope sampling processes. Importantly, the data used for parameter identification is directly extracted from the filtered digital signal within the digital controller, without undergoing the subsequent signal playback process. This approach avoids the influence of additional noise on the identification results.

Fig. 19 presents a comparison of the experimental data and the identified model for the three-phase currents i_{abc}. From the diagram, it can be observed that the experimental and identification waveforms exhibit strong agreement, demonstrating the high accuracy of the identification algorithm.

To verify the accuracy of the identification algorithm, a high-bandwidth, passive voltage probe (Tektronix TPP0250, 250 MHz) is employed to measure the IGBT ON-state voltage. Since the IGBT is enclosed within the PCS, the differential probe is connected between the dc voltage input terminal and the converter output terminal. The voltage probe has a measurement accuracy of ±2%. To further improve measurement accuracy during the experiment, the attenuation ratio of the voltage probe is set to a lower range when measuring the IGBT ON-state voltage. When the IGBT turns ON, the voltage across its terminals drops from high to low. Therefore, the oscilloscope trigger mode is set to falling edge triggering. In addition, the time base and vertical sensitivity of the oscilloscope are adjusted to enhance waveform resolution and display detail.

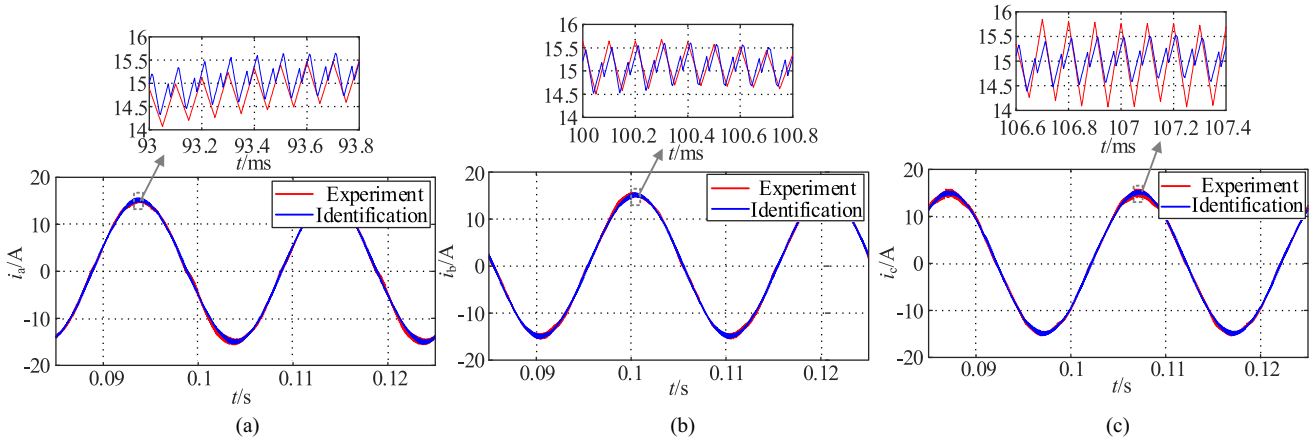

Fig. 19. Comparison of three-phase current data for experiment and identification model. (a) Waveforms comparison of phase A current at $i_{\mathrm{abc}} = 15$ A. (b) Waveforms comparison of phase B current at $i_{\mathrm{abc}} = 15$ A. (c) Waveforms comparison of phase C current at $i_{\mathrm{abc}} = 15$ A.

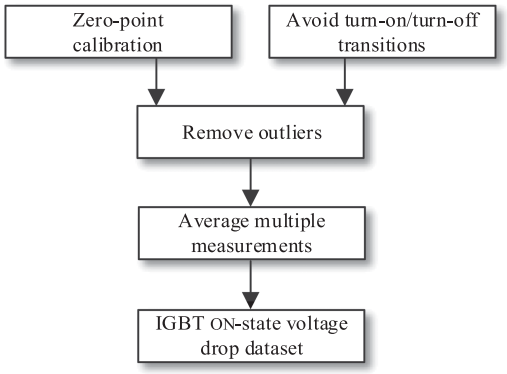

Fig. 20. Flowchart of ON-state voltage measurement.

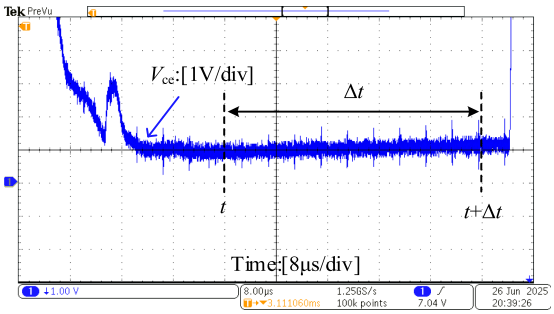

Fig. 21. Experiment results of the V_{ce} of IGBT.

Considering the relatively small magnitude of the ON-state voltage, conventional measurement methods may fail to achieve sufficient accuracy. To address this issue, this article proposes a high-precision measurement scheme, with the detailed procedure illustrated in Fig. 20. Prior to measurement, zero-offset calibration is performed on the measurement equipment to effectively reduce systematic errors.

In addition, to avoid interference from the Miller plateau and switching transients, the flat segment of the voltage waveform—24 μs to 32 μs after turn-ON—is selected for measurement, as shown in Fig. 21. Furthermore, statistical outlier removal is applied to improve data stability and consistency. To mitigate the impact of noise on the monitoring performance, the average value of 50 000 sampling points during the steady-state period of the ON-state voltage is taken as the final measurement result. On-state voltage values under various conduction currents are recorded. Several specific junction temperatures are selected, and repeated measurements are conducted to obtain ON-state voltage data across different current and temperature conditions.

TABLE V
PARAMETER IDENTIFICATION RESULTS

Number	V_{ce1}(V)	V_{ce3}(V)	V_{ce5}(V)
1	1.035	1.022	0.983
2	1.186	1.144	1.100
3	1.108	1.007	1.106
4	1.175	0.994	1.084
5	1.184	1.128	1.017
6	1.020	1.133	1.116
7	1.210	1.104	1.113
8	1.069	1.047	1.075
9	1.002	1.211	1.142
10	1.157	1.202	1.123
Average	1.115	1.099	1.086
Measured	1.068	1.143	1.124
Error	4.38%	3.85%	3.36%

*Conditions: 13th Gen Intel(R) Core(TM) i5-13400 2.50 GHz, 16-GB RAM, 64-bit system.

The ON-state voltage of IGBT with different collector current can be calculated according to (8) and (9). Table V provides the measured and identified ON-state voltage for the upper-arm IGBTs in the PCS three-phase system with a conduction current of 6 A. As shown, the identification error of the ON-state voltage of IGBT is within 5%. It is proved that the method can accurately identify the relevant parameters of ON-state voltage of IGBT, and the accuracy of the identification method is verified. Furthermore, by comparing with the initial ON-state voltage provided in Fig. 7, it can be seen that the operating IGBT module exhibits a higher ON-state voltage than its value at manufacture. This phenomenon indicates that, with the accumulation of operating time, the IGBT module has undergone a certain degree of aging, resulting in observable degradation of its electrical characteristics. These experimental results not only validate the correlation between IGBT aging and changes in the ON-state voltage but also

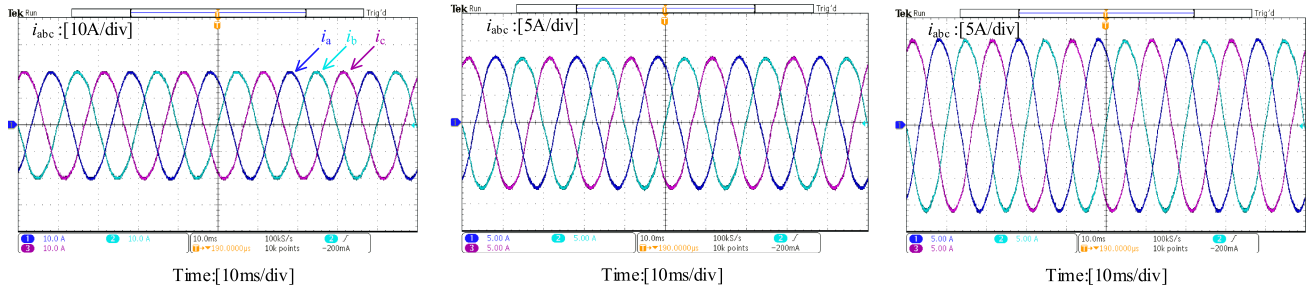

Fig. 22. Waveforms of PCS under different conditions. (a) $i_{\mathrm{abc}} = 20$ A. (b) $i_{\mathrm{abc}} = 12$ A. (c) $i_{\mathrm{abc}} = 16$ A.

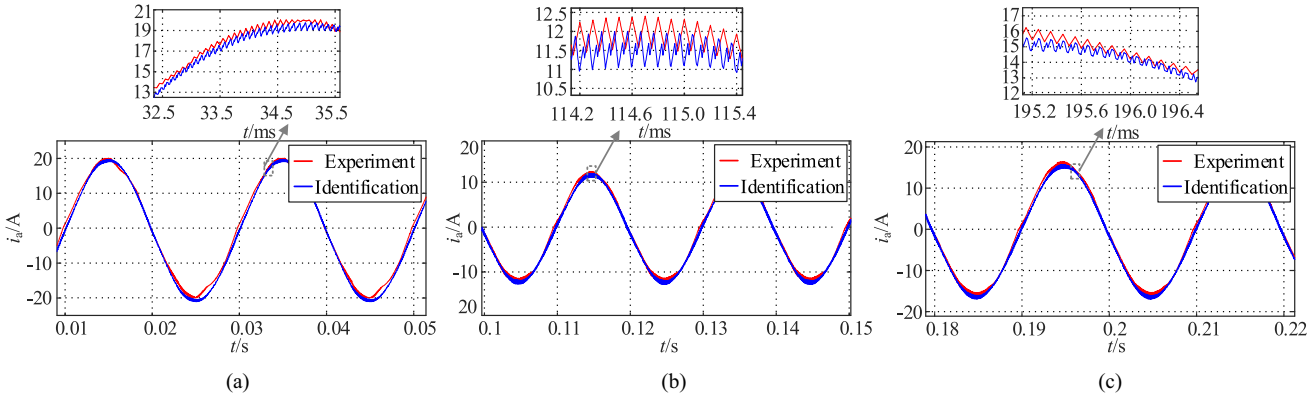

Fig. 23. Waveforms comparison of PCS under multiworking conditions. (a) Waveforms comparison of phase A current at $i_{\mathrm{abc}} = 20$ A. (b) Waveforms comparison of phase A current at $i_{\mathrm{abc}} = 12$ A. (c) Waveforms comparison of phase A current at $i_{\mathrm{abc}} = 16$ A.

demonstrate that the proposed condition monitoring algorithm can effectively capture the aging characteristics of the device. This highlights the significant engineering application value of the algorithm for assessing the health status of IGBT modules.

Since the output current of PCS is influenced by multiple factors including the energy storage power supply, grid voltage, control strategy, temperature, harmonics, and operation states, it exhibits dynamic variations rather than remaining constant. To further validate the robust parameter identification capability of the proposed condition monitoring algorithm and demonstrate its capability under industrial application, this article presents identification results for grid-connected currents of 12 A, 16 A, and 20 A.

Fig. 22 illustrates the experimental waveforms under different IGBT collector currents. As shown in Fig. 23, the established mathematical analytical model demonstrates excellent agreement with the output characteristics of the physical converter, highlighting the high accuracy of the identification model. This confirms that the model can be effectively utilized for IGBT condition monitoring.

Therefore, it is crucial to compare the identified parameters with the tested parameters to validate both the effectiveness of the proposed data preprocessing method and the accuracy of the identification algorithm.

Table VI provides the average values and errors of the monitoring results. Analysis of these results reveals that the monitoring error remains below 5%, which is within the acceptable error range. This confirms that the proposed monitoring algorithm can accurately identify the ON-state voltage of the IGBT under various operating conditions.

TABLE VI
ANALYSIS OF MONITORING RESULTS UNDER DIFFERENT GRID-CONNECTED CURRENTS

Case	V_{ce1}(V)	V_{ce3}(V)	V_{ce5}(V)
8 A	1.231	1.269	1.253
10 A	1.412	1.369	1.362
12 A	1.596	1.505	1.516
Max Err	4.28%	2.09%	1.17%

*Conditions: 13th Gen Intel(R) Core(TM) i5-13400 2.50 GHz, 16-GB RAM, 64-bit system.

TABLE VII
MONITORING RESULTS OF V_{CE} BEFORE AND AFTER TEMPERATURE CHANGES

Temperature	V_{ce1}(V)	V_{ce3}(V)	V_{ce5}(V)
45°C	1.187	1.173	1.181
60°C	1.110	1.140	1.086
Max Err	2.33%	1.56%	1.81%

*Conditions: 13th Gen Intel(R) Core(TM) i5-13400 2.50 GHz, 16-GB RAM, 64-bit system.

To further examine the accuracy of the condition monitoring algorithm, the ON-state voltage of the IGBT was measured at different temperatures with a current of 9 A. Data were collected at the initial startup and after a period of PCS operation. As shown in Table VII, the monitoring error is below 3%, demonstrating the algorithm's capability to effectively monitor the degradation of IGBTs.

TABLE VIII
PERFORMANCE COMPARISON OF DIFFERENT MONITORING METHODS

Method	Mean monitoring time	Memory	Parameter tuning complexity	Implementation cost	Noise robustness
PSO [27]	69.58 s	Medium	High	Low	Low
WOA [29]	66.78 s	Medium	High	Medium	Low
BP-NN [17]	Training: required Monitoring: fast	High	Medium	High	Medium
Proposed	9.34 s	Low	Low	Low	High

*PSO: particle swarm optimization; WOA: whale optimization algorithm; BP-NN: backpropagation neural network.

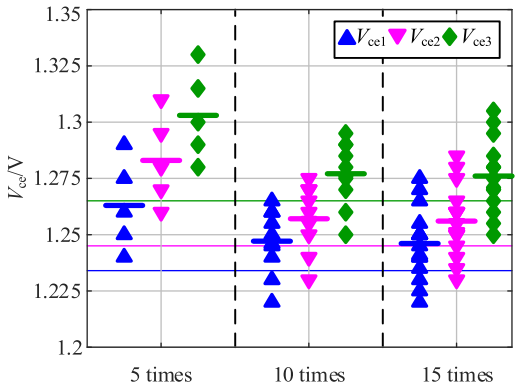

Fig. 24. V_{ce} identification results under different identification times.

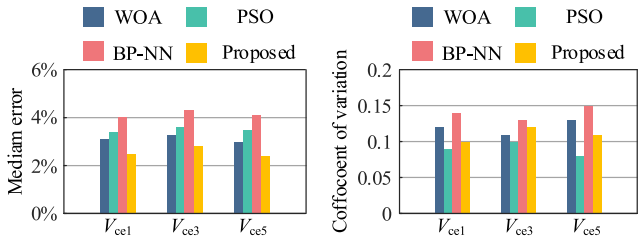

Fig. 25. Analysis of monitoring results under different algorithms.

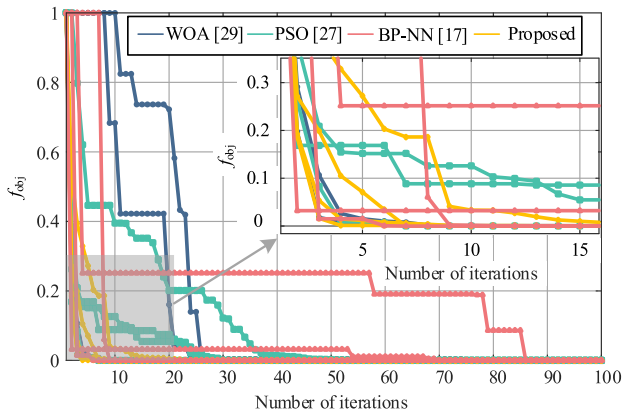

Fig. 26. Iterative process of different algorithms.

As shown in Fig. 24, increasing the number of repetitions can improve accuracy to some extent, but it also significantly increases computational time. Given that the IGBT aging process in practical applications takes much longer than the identification process, and taking into account computational resource usage and identification accuracy, 10 repetitions provide a reasonable balance between precision and efficiency. Therefore, the authors have adopted 10 repeated identifications as the standard approach throughout the article.

It should be noted that the condition monitoring algorithm proposed in this article still presents a certain degree of model error in the identification results. One reason is that the established mathematical analytical model does not account for parasitic parameters introduced by wiring in the actual system, which may interfere with the accuracy of IGBT ON-state voltage identification. However, considering their relatively small magnitude and minimal impact on the recognition of health parameter trends, these parasitic effects are neglected in the modeling process. In addition, the inherent randomness of the algorithm itself can also introduce some error into the monitoring results.

C. Performance Comparison of the Proposed Method

To validate the effectiveness and superiority of the proposed method, this article designs a comparative experiment. Table VIII compares the proposed nonlinear least squares-based approach with existing condition monitoring methods, including PSO-based methods [27], WOA [29], and a backpropagation neural network (BP-NN) based method [17]. These approaches represent current state-of-the-art techniques and are selected as benchmark solutions for a comprehensive comparative analysis.

These methods are computed in MATLAB on a computer (Intel Core i5-13400 @2.5 GHz, 16-GB RAM, 64-bit system). The test conditions are listed in the simulation column of Table VIII and each method is repeated ten times. The comparison focuses on computation time, accuracy, noise robustness, implementation cost. BP-NN requires a large dataset for training and must be executed on a computer. The proposed condition monitoring algorithm has low computational complexity, needs less data, and runs quickly. It can be deployed on a DSP.

As shown in Fig. 25, the results indicate that the nonlinear least squares method is less prone to becoming trapped in local optima, resulting in lower errors. The low coefficient of variation (CV) further suggests that the proposed condition monitoring algorithm has the ability to escape local optima. Since optimization algorithms inherently involve some randomness, the nonlinear least squares method may occasionally fall into local optima. However, the monitoring accuracy and CV performance of the IGBT key parameters remain stable, demonstrating the algorithm's good robustness and accuracy.

Fig. 26 compares the iterative processes of the three algorithms, and it can be observed that under the same number of

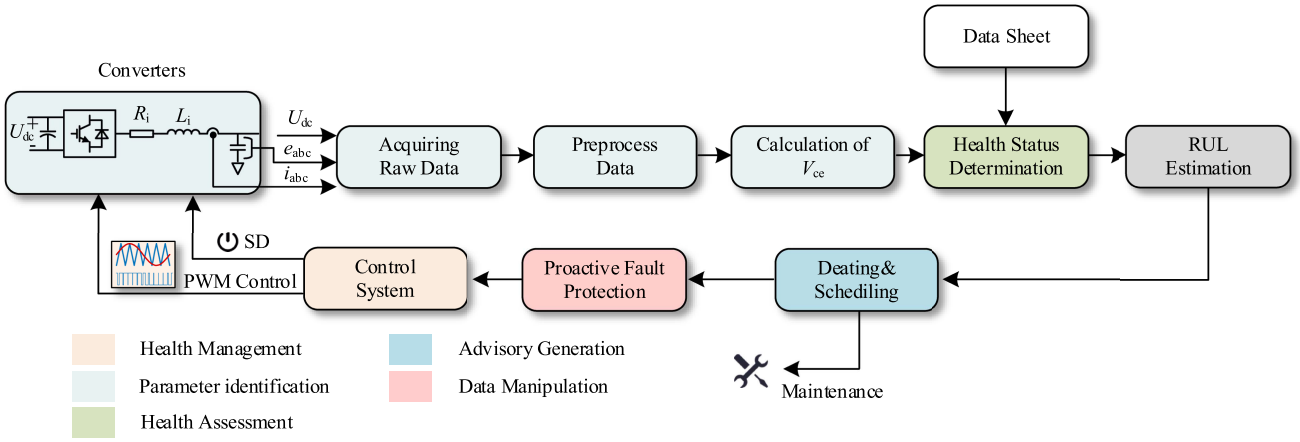

Fig. 27. Workflow of the proposed IGBT monitoring method and its integration with existing control strategies.

iterations, the TRRLS algorithm achieves a smaller error and exhibits faster convergence speed.

VI. Discussions and Potentials

As shown in Fig. 27, the proposed IGBT monitoring method demonstrates a certain level of integrability and is compatible with existing control strategies such as lifetime estimation and active fault protection. The method uses transient data, such as dc voltage and ac-side inductor current, as inputs, which can be directly obtained from the control feedback signals without requiring additional hardware. This makes the approach suitable for implementation in embedded systems. The model can be continuously updated during operation to adapt to long-term aging trends.

This monitoring method enables continuous extraction of key aging-related parameters, providing essential input for both data-driven and physics-based lifetime estimation models. It supports real-time updates of the remaining useful lifetime prediction under dynamic operating conditions.

Furthermore, by detecting abnormal fluctuations or degradation trends in electrical parameters in real time, the method can serve as a trigger for active fault protection mechanisms. For example, upon detecting a rapid increase in ON-state voltage, the system can initiate derating, activate thermal control, or switch to redundant modules proactively. Therefore, the proposed method can be integrated into existing control frameworks to extend device lifespan and enhance system reliability.

VII. Conclusion

In this article, a mathematical analytical model of a three-phase two-level PCS is established, and a nonlinear least squares based condition monitoring method for the ON-state voltage of IGBTs is proposed. Additionally, considering the presence of measurement noise in sensor sampling signals in practical engineering applications, the collected data undergoes preprocessing. A multisensor data fusion approach combined with a Kalman filtering algorithm is employed to minimize data deviations and noise interference. The correctness and effectiveness of the proposed IGBT condition monitoring method is verified through simulations and experiments under various operating conditions. The advantages of the proposed condition monitoring method are summarized as follows:

1) The nonlinear least squares algorithm using the trust-region reflective method is experimentally verified to ensure the monitoring strategy's accuracy.
2) Integrating the energy storage converter model with a Kalman filter effectively mitigates the impact of sensor sampling noise on IGBT parameter identification.
3) From an industrial application perspective, condition monitoring can be achieved using existing sensors, without additional sensors, noninvasive, and able to accurately monitor the IGBT aging relevant parameters.
4) The proposed method enables the creation of a precise discrete simulation model of the converter based on experimental data. This model can be applied to other types of converters, facilitating further research and development.

References

[1] K. Yan, G. Li, R. Zhang, Y. Xu, T. Jiang, and X. Li, "Frequency control and optimal operation of low-inertia power systems with HVDC and renewable energy: A review," *IEEE Trans. Power Syst.*, vol. 39, no. 2, pp. 4279–4295, Mar. 2024.

[2] J. Wang, K. Sun, C. Xue, T. Liu, and Y. Li, "Multi-port DC-AC converter with differential power processing DC-DC converter and flexible power control for battery ESS integrated PV systems," *IEEE Trans. Ind. Electron.*, vol. 69, no. 5, pp. 4879–4889, May 2022.

[3] H. Wang and F. Blaabjerg, "Power electronics reliability: State of the art and outlook," *IEEE J. Emerg. Sel. Topics Power Electron.*, vol. 9, no. 6, pp. 6476–6493, Dec. 2021.

[4] S. Zhao, F. Blaabjerg, and H. Wang, "An overview of artificial intelligence applications for power electronics," *IEEE Trans. Power Electron.*, vol. 36, no. 4, pp. 4633–4658, Apr. 2021.

[5] J. Falck, C. Felgemacher, A. Rojko, M. Liserre, and P. Zacharias, "Reliability of power electronic systems: An industry perspective," *IEEE Ind. Electron. Mag.*, vol. 12, no. 2, pp. 24–35, Jun. 2018.

[6] Y. Yang and P. Zhang, "In situ junction temperature monitoring and bond wire detecting method based on IGBT and FWD on-state voltage drops," *IEEE Trans. Ind. Appl.*, vol. 58, no. 1, pp. 576–587, Jan./Feb. 2022.

[7] U.-M. Choi, F. Blaabjerg, S. Jørgensen, S. Munk-Nielsen, and B. Rannestad, "Reliability improvement of power converters by means of condition monitoring of IGBT modules," *IEEE Trans. Power Electron.*, vol. 32, no. 10, pp. 7990–7997, Oct. 2017.

[8] L. Rossetto and G. Spiazzi, "A fast ON-state voltage measurement circuit for power devices characterization," *IEEE Trans. Power Electron.*, vol. 37, no. 5, pp. 4926–4930, May 2022.

[9] Y. Peng, Y. Shen, and H. Wang, "A converter-level on-state voltage measurement method for power semiconductor devices," *IEEE Trans. Power Electron.*, vol. 36, no. 2, pp. 1220–1224, Feb. 2021.
[10] T. Poller, J. Lutz, B. Böttge, and H. Knoll, "Analysis of the plastic deformation in aluminium metallizations of Al2O3-based DAB substrates," in *Proc. 15th Eur. Conf. Power Electron. Appl.*, Lille, 2013, pp. 1–10.
[11] M. Ciappa, "Selected failure mechanism of modern power modules," *Microelectron. Rel.*, vol. 42, no. 4/5, pp. 653–667, Apr./May 2002.
[12] B. Yao, Y. Peng, Y. Zhang, H. Wang, and H. Wang, "An estimation method of high-order LC circuits in power electronic converters," *IEEE Trans. Ind. Electron.*, vol. 71, no. 5, pp. 5274–5284, May 2024.
[13] J. Miao, Y. Liu, Q. Yin, B. Ju, G. Zhang, and H. Wang, "A novel soft fault detection and diagnosis method for a DC/DC buck converter based on contrastive learning," *IEEE Trans. Power Electron.*, vol. 39, no. 1, pp. 1501–1513, Jan. 2024.
[14] X. Wei, B. Yao, Y. Peng, Y. Sun, K. Wang, and H. Wang, "An improved discharge profile-based DC-link capacitance estimation for traction inverter in electric vehicle applications," *IEEE Trans. Power Electron.*, vol. 39, no. 7, pp. 8696–8708, Jul. 2024.
[15] S. Chen, S. Ji, L. Pan, C. Liu, and L. Zhu, "An on-state voltage calculation scheme of MMC submodule IGBT," *IEEE Trans. Power Electron.*, vol. 34, no. 8, pp. 7996–8007, Aug. 2019.
[16] S. Zhao, Y. Peng, Y. Zhang, and H. Wang, "Parameter estimation of power electronic converters with physics-informed machine learning," *IEEE Trans. Power Electron.*, vol. 37, no. 10, pp. 11567–11578, Oct. 2022.
[17] Z. She, Y. Liu, W. Cao, and G. Chen, "Full-parameter identification of buck converter through BP-NN fitting explicit time-domain relationships," *IEEE Trans. Power Electron.*, vol. 39, no. 6, pp. 7560–7571, Jun. 2024.
[18] Y. Peng, S. Zhao, and H. Wang, "A digital twin based estimation method for health indicators of DC–DC converters," *IEEE Trans. Power Electron.*, vol. 36, no. 2, pp. 2105–2118, Feb. 2021.
[19] S. Zhang, W. Song, H. Cao, T. Tang, and Y. Zou, "A digital-twin-based health status monitoring method for single-phase PWM rectifiers," *IEEE Trans. Power Electron.*, vol. 38, no. 11, pp. 14075–14087, Nov. 2023.
[20] H. Shi, L. Xiao, Q. Wu, and W. Wang, "Digital twin approach for IGBT parameters identification of a three-phase DC-AC inverter," in *Proc. IEEE Transp. Electrific. Conf. Expo Asia-Pacific*, 2022, pp. 1–4.
[21] Y. Liu, Y. Wang, N. Zhang, D. Lu, and C. Kang, "A data-driven approach to linearize power flow equations considering measurement noise," *IEEE Trans. Smart Grid*, vol. 11, no. 3, pp. 2576–2587, May 2020.
[22] Y. Peng, K. Wang, X. Wei, Z. Shuai, and H. Wang, "An online converter-level wear-out failure mode separation method for power semiconductor devices," *IEEE Trans. Ind. Electron.*, vol. 72, no. 4, pp. 4218–4226, Apr. 2025.
[23] W. Song, Y. Zou, C. Ma, and S. Zhang, "Digital twin modeling method of three-phase inverter-driven PMSM systems for parameter estimation," *IEEE Trans. Power Electron.*, vol. 39, no. 2, pp. 2360–2371, Feb. 2024.
[24] T. M. Le, B. Fatahi, H. Khabbaz, and W. Sun, "Numerical optimization applying trust-region reflective least squares algorithm with constraints to optimize the non-linear creep parameters of soft soil," *Appl. Math. Model.*, vol. 41, pp. 236–256, Jan. 2017.
[25] Z. Zhang, L. Liang, L. Tu, and Z. Zhang, "An online junction temperature monitoring method for press-pack IGBT based on a novel TSEP with a good linearity," *IEEE Trans. Power Electron.*, vol. 40, no. 5, pp. 6829–6837, May 2025.
[26] A. Moazami, S. Mohsenzade, and K. Akbari, "An online condition monitoring method for IGBT gate oxide degradation based on the gate current in Miller Plateau," *IEEE Trans. Ind. Electron.*, vol. 70, no. 9, pp. 9505–9514, Sep. 2023.
[27] W. Song, Z. Zhang, S. Zhang, C. Ma, and J. Li, "Digital twin modeling and multi-parameter monitoring schemes of three-level ANPC inverters," *IEEE Trans. Power Electron.*, vol. 39, no. 12, pp. 16596–16608, Dec. 2024.
[28] S. Ou, S. Sahoo, A. Sangwongwanich, Y. Liu, and F. Blaabjerg, "A sensor-less IGBT on-state voltage estimation method using inverter control variables," in *Proc. IEEE Appl. Power Electron. Conf. Expo.*, Atlanta, GA, USA, 2025, pp. 1501–1506.
[29] M. Mafarja and S. Mirjalili, "Whale optimization approaches for wrapper feature selection," *Appl. Soft. Comput.*, vol. 62, pp. 441–453, Jan. 2018.

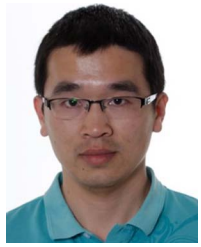

Yanjun Tian (Member, IEEE) received the B.Sc. and M.Sc. degrees in electrical engineering from Yanshan University, Qinhuangdao, China, in 2009 and 2012, respectively, and the Ph.D. degree in power electronics from Aalborg University, Aalborg, Denmark, in 2016.

He is currently an Associate Professor with North China Electric Power University, Baoding, China. His research interests include distributed generation and power converter control, focusing on the impedance interaction, stability control, data driven modeling, and situational awareness.

Shaopeng Song (Student Member, IEEE) was born in Hebei Province, China, in 2000. He received the B.Sc. degree in electrical engineering from Hebei Agricultural University, Baoding, China, in 2023. He is currently working toward the master's degree with North China Electric Power University, Baoding.

His research interests include the failure mechanisms analysis of power electronic components,focusing on improving of the robustness and reliability of power converters through condition monitoring.

Xiaoqi Xu (Student Member, IEEE) was born in Jiangsu Province, China, in 2000. He received the B.Sc. degree in electrical engineering from Yangzhou University, Yangzhou, China, in 2022. He is currently working toward the Ph.D. degree in the stable and optimal control of grid-forming converters with North China Electric Power University, Baoding, China.

His research interests include distributed generation and grid-forming control, focusing on the stability analysis and stability-enhancing control of grid-forming converters.